RESEARCH ARTICLE

Imaging Cloaked Objects: Diffraction Tomography of Realistic Invisibility Devices

Francisco J. Díaz-Fernández,* Javier Martí, and Carlos García-Meca*

Invisibility cloaks have become one of the most outstanding developments among the wide range of applications in the field of metamaterials. So far, most efforts in invisibility science have been devoted to achieving practically realizable cloak designs and to improving the effectiveness of these devices in reducing their scattering cross-section (SCS), a scalar quantity accounting for the total electromagnetic energy scattered by an object. However, little attention has been paid to the opposite side of the technology: the development of more efficient techniques for the detection of invisibility devices. For instance, the SCS ignores the phase change introduced by the cloak, as well as the angular dependence of the incident and scattered waves. Here, a different path is proposed, which takes advantage of the smarter way in which diffraction tomography processes all this overlooked information to improve the efficiency in unveiling the presence of invisibility devices. This approach not only results in a considerable sensitivity enhancement in the detection of different kinds of cloaks based on both scattering cancellation and transformation optics, but also enables us to obtain images depicting the approximate shape and size of the cloak. The proposed method can be extended to the detection of sound cloaks.

1. Introduction

Invisibility has been one of the most challenging effects pursued by humankind for centuries. The possibility of hiding objects to the naked eye has recently leaped from science fiction to a feasible reality thanks to the advent of metamaterials.[1] Among a

F. J. Díaz-Fernández, J. Martí
Nanophotonics Technology Center
Universitat Politècnica de València
Valencia 46022, Spain
E-mail: fradafer@ntc.upv.es
J. Martí, C. García-Meca
Research Area
DAS Photonics S.L.
Valencia 46022, Spain
E-mail: cgarcia@dasphotonics.com

wide range of applications that arises through the exploitation of this kind of materials not available in nature, invisibility cloaks are one of the most high-impact developments.[2,3] The impressive ability of these devices to hide objects by reducing the scattering they produce has even been experimentally demonstrated,[4,5] boosting the impact of this field of study over the last two decades. Different approaches to the achievement of invisibility have followed in different fields besides optics. For instance, a variety of cloaking devices have been experimentally demonstrated also in acoustics, thermodynamics, and mechanics.[6] However, cloaking devices are not perfect. It has been shown that outside the design frequency, realistic cloaks may become significantly visible.[7] Conversely, as technology improves, detecting a cloak at the design frequency might be a challenging task. In most previous studies, the scattering cross section (SCS) has been used as an indicator of the effectiveness of realistic invisibility cloaks.[7–9] The SCS is a measurement that estimates the total energy scattered by an object (see Experimental section). Therefore, the use of this scalar value has the disadvantage that it does not take into account the spatial distribution of the scattered field nor the phase changes produced by the cloak and, in the case of devices without rotational symmetry, only a single illumination direction is usually considered. It is thus reasonable to imagine that a suitable measurement and processing of these missing data would provide more information on the cloak, which, as predicted in ref. [7], should be more sensible to interferometric techniques than to the SCS. Actually, looking back at the origins of invisibility cloaks, we find that one of the first known invisibility devices was conceived as a material undetectable by tomographic techniques,[10] which aim at reconstructing the refractive index (RI) profile of an object by illuminating it from each possible direction and by smartly combining the complex amplitude (magnitude and phase) of the resulting scattered waves.[11] Therefore, diffraction tomography (DT) is expected to detect invisibility devices more accurately, and even has the potential of revealing the shape of the cloak (see **Figure 1**).

In this paper, we explore this possibility, keeping the spotlight on studying the behavior of passive cloaks under DT around their design frequency, at which the SCS measurement is less effective and may fail to unveil their presence. Particularly, we analyze three of the most representative kinds of invisibility
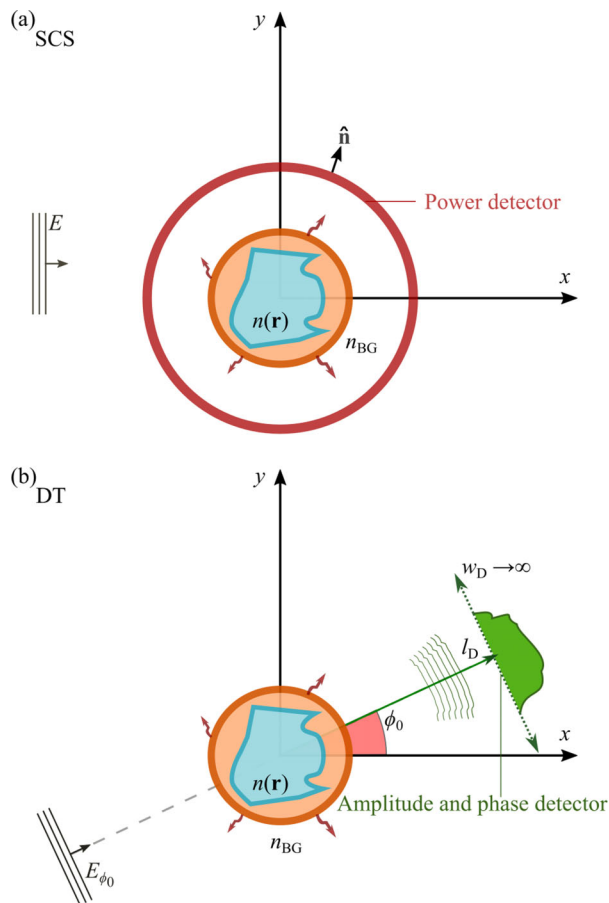
Figure 1. Scheme of the difference between the SCS and DT detection techniques. a) The SCS is a scalar quantity related to the total scattered power for a given incident direction. The phase of the scattered field is not taken into account. b) DT uses different angles of illumination to obtain a RI map of the object from the space-dependent phase and amplitude of the scattered field.

devices: plasmonic cloaks based on scattering cancellation (SC), blow-up-a-point inhomogeneous cloaks based on transformation optics (TO), and homogeneous polygonal cloaks, also based on TO (see **Figure 2**).

In all cases, we consider realistic material implementations. Additionally, it is worth mentioning that DT is constrained by the diffraction limit, that is, it is suited for imaging objects with dimensions larger than $\lambda/2$, where λ is the wavelength of light, if both the forward and backward scattering are measured. If the latter is not considered, which is the common situation and the one we will consider in this work, the limit rises to $\lambda/\sqrt{2}$,[12] so we will restrict our study to this class of objects. Moreover, we will focus on 2D problems for simplicity, although the extension to the 3D case is straightforward. Likewise, we restrict ourselves to TE waves (electric field polarized along the z component and magnetic field contained in the XY plane), with analogous results for TM waves.

Finally, to implement the DT algorithms used in this paper, the steps described in refs. [12, 13] have been coded in MATLAB. These robust algorithms have been used, for example, to measure the refractive index of a single cell.[14]
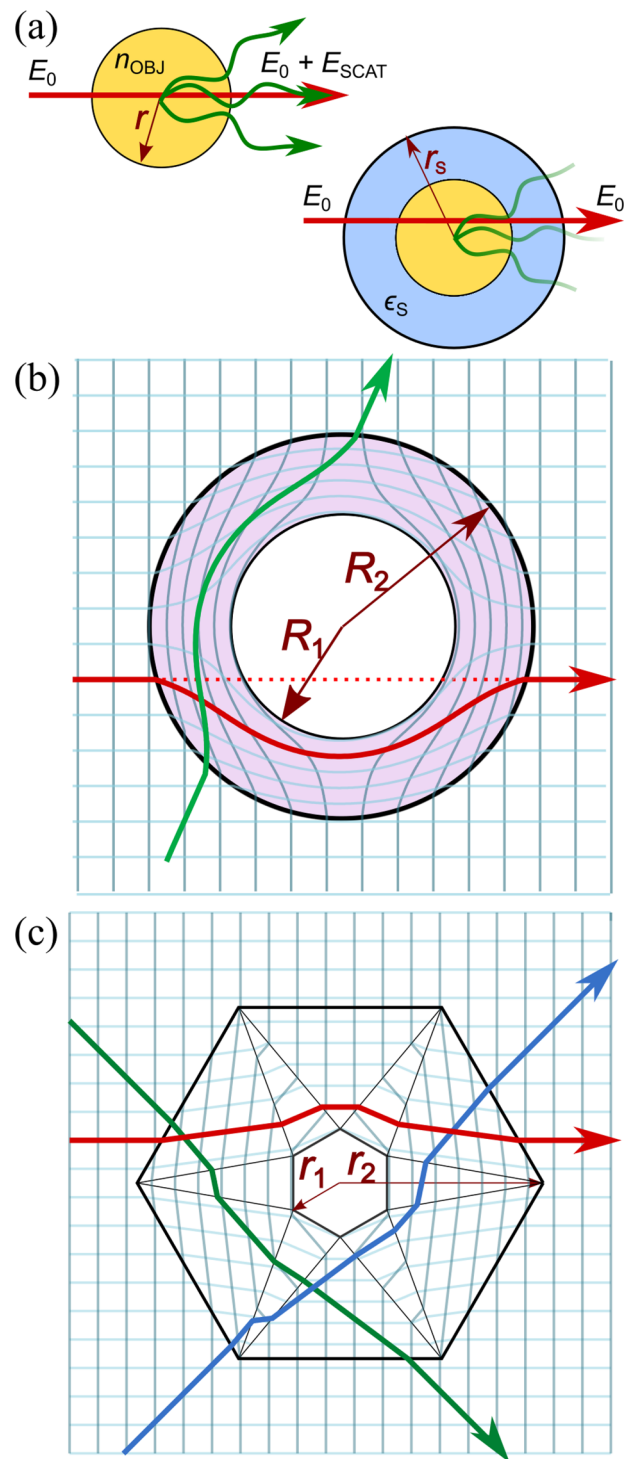

Figure 2. Studied invisibility cloaks and their working principle. a) SC cloak. b) Blow-up-a-point TO cloak. c) Polygonal TO cloak.

2. Results and Discussion

2.1. Scattering Cancellation

The first approach to invisibility cloaking that we will study is scattering cancellation. This technique reduces the scattering
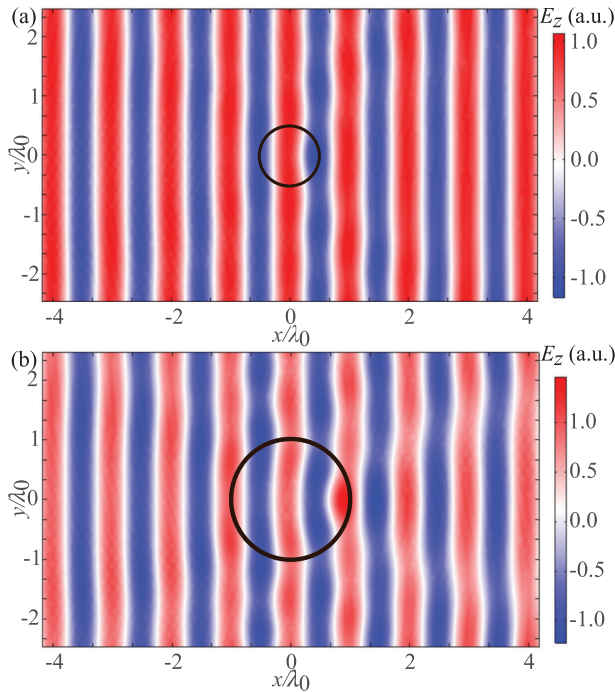
Figure 3. Simulated z component of the electric field resulting from the illumination of a SC-cloaked dielectric cylinder of radius r with an x-directed plane wave. a) $r = \lambda_0/2$. b) $r = \lambda_0$.

produced by a dielectric object with a positive permittivity by covering it with a negative-permittivity coating (see Figure 2a).[8] SC has also been applied to cloak objects immersed in a uniform static magnetic field[15] or in a diffusive light scattering medium.[16] An interesting application of this type of cloak is the possibility of cloaking a sensor without affecting its capability to measure an incoming signal.[17] Typically, the SC set-up consists of a core–shell spherical or cylindrical structure in which the oppositely signed permittivities of the inner and outer materials are designed to cancel the first-order scattered field at a given frequency (the design frequency).[8] Note that the SC effect is maximized for objects with electrically small dimensions.[8] Therefore, taking into account the diffraction limit of DT, we will analyze objects with longitudinal dimensions in the interval $[\lambda_0/\sqrt{2}, 2\lambda_0]$, where λ_0 is the free-space wavelength for which the cloaks are designed, with f_0 the corresponding frequency. Moreover, to satisfy the Born and Rytov approximations usually employed in DT,[12,18] the maximum contrast between the object RI and that of the background is fixed to a 5%. In particular, we apply the SC technique to cloak dielectric cylinders of radii $\lambda_0/2$ and λ_0, with a RI $n_{\text{OBJ}} = 1.05$, and immersed in a vacuum background with RI $n_{\text{BG}} = 1$. These cloaks have been optimized to minimize the SCS following the procedure described in ref. [19] (see Appendix 4). This yields optimum metallic shells with a permittivity $\epsilon_s = -2.7$ and an outer radius $r_s = 0.508\lambda$ for the $r = \lambda_0/2$ cylinder and $r_s = 1.0205\lambda_0$ for the $r = \lambda_0$ cylinder. As mentioned above, the electric field is assumed to be polarized along the z component (parallel to the cylinder axis). **Figure 3** shows the distribution of this field for both studied SC cloaks under plane wave incidence.

To quantify the effectiveness of the cloak in terms of the SCS reduction it attains, we define the relative observability as

$$O_{\text{SCS}} = \frac{\text{SCS}_{\text{C}}}{\text{SCS}_{\text{NC}}} \tag{1}$$

where SCS_{C} and SCS_{NC} are the SCS of the object with and without cloak, respectively. That is, the lower the value of O_{SCS}, the higher the efficiency of the cloak. In the case of the $r = \lambda_0/2$ cylinder, a value of $O_{\text{SCS}} = 0.7$ is achieved, while for the $r = \lambda_0$ cylinder, $O_{\text{SCS}} = 0.66$.

On the other hand, to obtain tomographic images (called *tomograms*) of all the cloaks studied in this work, the scattered field is recorded on a detector line (this data set is called a *projection*) placed at a distance l_{D} from the set-up center, as shown in Figure 1b. In the case of the SC cylinders, we set $l_{\text{D}} = 10\lambda_0$. Ideally, the detector line should be infinite to capture the complete forward scattered wave. In practice, in the simulations we use a finite line length w_{D} such that the missed scattered field is negligible. In the case of the SC cylinders, $w_{\text{D}} = 220\lambda_0$. A tomogram is built upon the information provided by different projections corresponding to different values of the illumination angle ϕ_0 (see Figure 1b). To ensure a nearly perfect tomographic quality, we take 250 projections and, at least, record the field of each projection at eight points per λ (a total of 1760 points in this case).

The obtained tomograms for the non-cloaked cylinders are shown in **Figure 4**, yielding a good approximation to the original cylinder RI profiles. It is worth mentioning that the reconstructed RI has a smooth variation instead of the abrupt RI change of the original cylinders, as we can see in Figure 4b,d. These results are in line with those expected for the tomography of a centered cylinder.[18] Notably, the RI recovered by the tomogram for the cloaked $r = \lambda_0/2$ configuration (Figure 4b) exhibits a higher amplitude variation than that of the non-cloaked configuration (0.1 with cloak, 0.06 without it). This increment of the RI range is more evident for the $r = \lambda_0$ cylinder, as can be seen in Figure 4d. Additionally, in this case, the RI profile shows two lobes instead of one. Regardless, the tomograms clearly show the presence of an object in both cases.

Following the work in ref. [7], it is worth analyzing the behavior of the cloak under DT at different frequencies. For that, the cloak was considered to be made of lossless silver,[7] and was modeled by a Drude permittivity $\varepsilon_s = \varepsilon_\infty - f_P^2/f^2$, with a plasma frequency $f_P = 2175$ THz and $\varepsilon_\infty = 5$.[20] As a consequence, the ideal cloak permittivity is obtained at $f_0 = 783.8$ THz (i.e., $\lambda_0 = 382.7$ nm). To quantify the sensitivity of DT in the detection of a given cloak, we define the presence of an object according to its tomogram as

$$p = \frac{\sum_{i=1}^{I} \sum_{j=1}^{J} |n_{\text{DT}}(i,j) - n_{\text{BG}}|}{IJ} \tag{2}$$

where $n_{\text{DT}}(i,j)$ is the RI at the pixel (i,j) of a tomogram of size $I \times J$. This is similar to the way in which the error of tomographic techniques is tested.[18] As in the case of the SCS, the effect of the cloak is quantified as the presence of the cloaked object divided by the presence of the non-cloaked one, that is

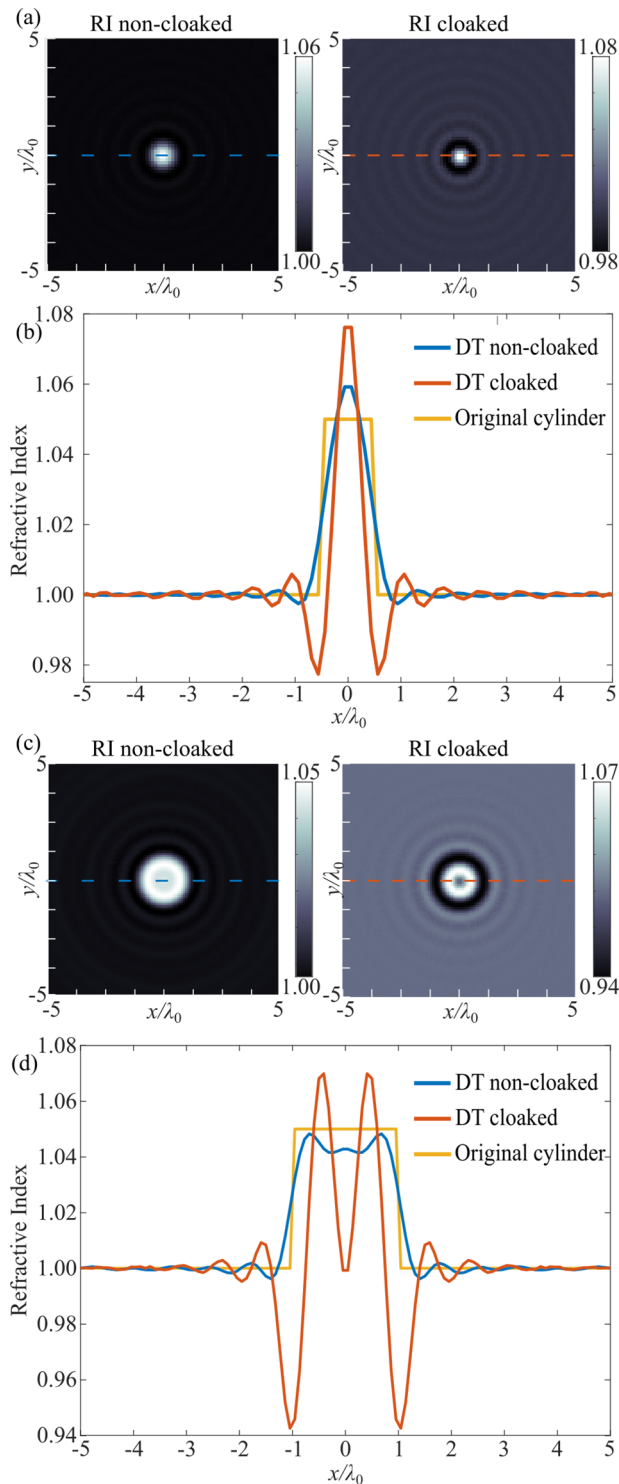$$O_{\text{DT}} = \frac{p_{\text{C}}}{p_{\text{NC}}} \tag{3}$$

Figure 4. Linear tomography (Rytov approximation) of non-cloaked and cloaked dielectric cylinders of radius a,b) $r = \lambda_0/2$ and c,d) $r = \lambda_0$. Full tomograms are shown in panels (a) and (c). Panels (b) and (d) show a detail of the RI along the dashed lines depicted in (a) and (c).
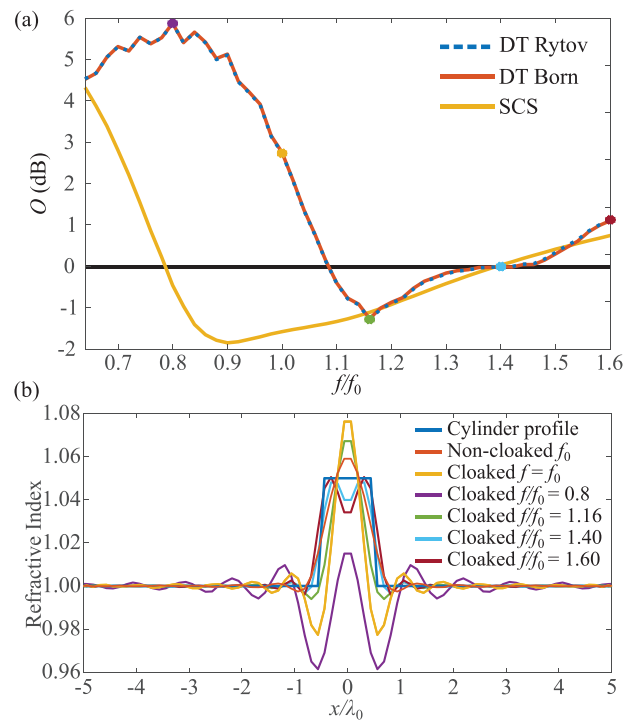

Figure 5. a) Comparison between the relative observabilities obtained via SCS and DT for an SC-cloaked cylinder with $r = \lambda_0/2$ and $n_{OBJ} = 1.05$ as a function of frequency. b) Corresponding RI along a line passing through the center of the cylinder as retrieved via DT for some selected frequencies (highlighted with colored points in (a)).

The detection ability of both measurement methods (SCS and DT) is shown in **Figure 5**a for $r = \lambda_0/2$ cylinder. The corresponding tomogram profiles along a line passing through the center of the cloak are shown in Figure 5b for some selected frequencies. As expected, O_{SCS} shows a local minimum close to $f = f_0$, since f_0 is the design frequency. As noted in ref. [7], there is a frequency range around f_0 for which the cloak reduces the scattering produced by the concealed object (that is, $O_{SCS} < 1$ or, equivalently, $O_{SCS} < 0$ dB), while the SCS is higher for the cloaked object in the rest of the spectrum ($f < 0.8f_0$ and $f > 1.4f_0$ in our case), as can be seen in Figure 5a. This corresponds to the values greater than 0 dB in this figure, which represent the frequencies at which the cloak not only fails at hiding the object, but enhances its presence, making it more detectable. Remarkably, in the eyes of DT, the presence of the cloaked system is almost always greater than that of the non-cloaked one in the studied band, even at the frequencies for which the cloak reduces the object SCS. Additionally, we have $O_{DT} \geq O_{SCS}$, so we conclude that DT will be more effective in discovering objects hidden by SC cloaks.

Besides allowing a presence measurement, DT provides information on the apparent shape of the cloaked object. In the tomograms of the studied cylinders, they appear to have a smaller radius and a larger RI variation than their bare counterparts (Figure 4). Consequently, we ask ourselves whether it would be possible to take advantage of this apparent shrinking, which suggests that covering small dielectric particles with SC coatings may facilitate their differentiation when being closely packed. To study this possibility, we analyze a new configuration consisting of two
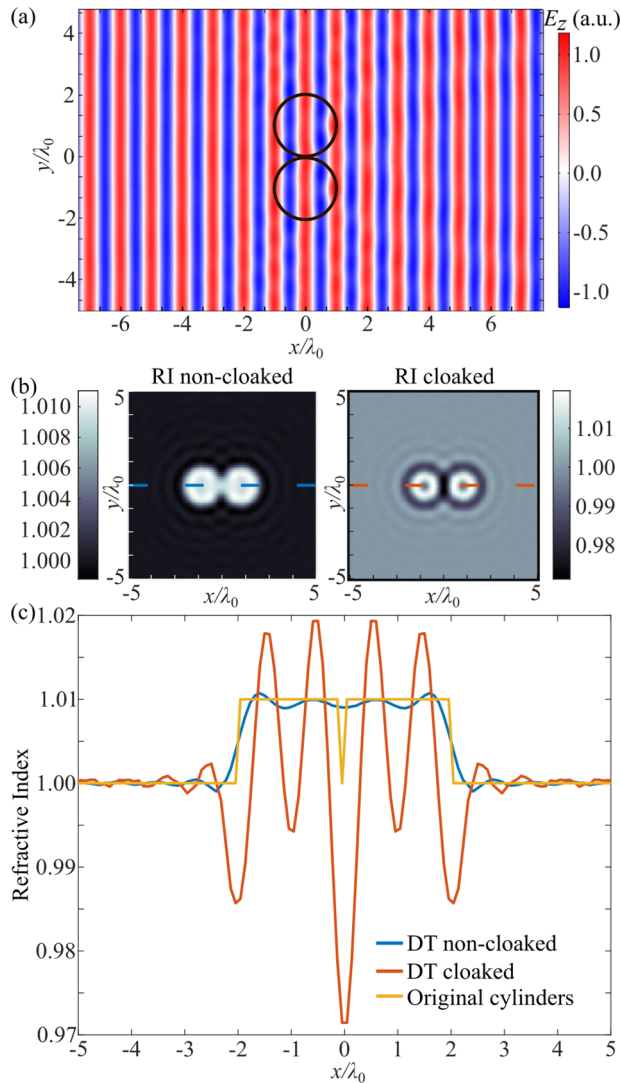
**ADVANCED
SCIENCE NEWS**

www.advancedsciencenews.com

LASER
& PHOTONICS
REVIEWS

www.lpr-journal.org

Figure 6. a) Simulated z component of the electric field resulting from the illumination of two SC-cloaked cylinders ($r = \lambda$) with an x-directed plane wave. b) Tomograms of the non-cloaked and cloaked cylinders obtained via DT (Rytov approximation). c) Detail of the RI along the dashed lines depicted in (b).

maximum RI values, provides a notable advantage in the recognition of closely packed objects, which may find application, for instance, in particle counting or bioimaging.

2.2. Transformation Optics - Blow-Up-A-Point Cloaks

A more sophisticated passive cloaking technique that can remove scattering at all orders is based on transformation optics.[3,21] With this method, a given region of space is hidden by redirecting the illuminating wave around it, avoiding any light absorption or scattering. The rays traversing the cloak bypass the concealed region and turn back to the original path. To study the behavior of this kind of device under DT, we analyze the original 2D cloak proposed in refs. [4, 22], where a cylindrical region of radius R_1 is hidden by a concentric cylindrical shell of radius R_2 (see Figure 2b). This cloak requires the following radius-dependent, anisotropic relative permittivity (ϵ), and permeability (μ) tensor components (in cylindrical coordinates)

$$
\epsilon_r = \mu_r = \frac{r - R_1}{r}
$$

$$
\epsilon_\phi = \mu_\phi = \frac{r}{r - R_1} \tag{4}
$$

$$
\epsilon_z = \mu_z = \left(\frac{R_2}{R_2 - R_1} \right)^2 \frac{r - R_1}{r}
$$

To account for causality and losses, we analyze a realistic version of the cloak in which the components with values below unity (ϵ_r, μ_r, ϵ_z, μ_z) are modeled by Drude and Lorentz dispersive relations, respectively[7,23]

$$
\epsilon_{rD}(\mathbf{r}) = \epsilon_r(\mathbf{r}) \left(2 - \frac{f_0^2}{f(f + i\gamma_1)} \right) \tag{5}
$$

$$
\epsilon_{zD}(\mathbf{r}) = \epsilon_z(\mathbf{r}) \left(2 - \frac{f_0^2}{f(f + i\gamma_1)} \right) \tag{6}
$$

$$
\mu_{rL}(\mathbf{r}) = \mu_r(\mathbf{r}) \left(1 - \frac{F}{1 + (i\gamma_2/f) - (f_0^2/f^2)} \right) \tag{7}
$$

$$
\mu_{zL}(\mathbf{r}) = \mu_z(\mathbf{r}) \left(1 - \frac{F}{1 + (i\gamma_2/f) - (f_0^2/f^2)} \right) \tag{8}
$$

For the components larger than unity (ϵ_ϕ, μ_ϕ), we assume a non-dispersive dependence,[7,23] given in our case by Equation (4). Following ref. [23], we take $\gamma_1 = \gamma_2 = \gamma$ and $F = 0.78$.

To validate this TO device, we simulate its response when cloaking a dielectric disk of radius $r_D = R_1$ and with a refractive index $n_{OBJ} = 1.04$. A design frequency $f_0 = 193.55$ THz (corresponding to a wavelength $\lambda_0 = 1.55$ μm) is chosen, and the dimensions of the cloak are taken to be $R_1 = 2$μm and $R_2 = 2R_1$.

kissing cloaked cylinders ($r = \lambda$, $n_{OBJ} = 1.01$), immersed in a vacuum background ($n_{BG} = 1$) and covered by optimized shells with $\epsilon_S = -2$ and $r_S = 1.0049\lambda$. The simulation of the corresponding electric field is shown in **Figure 6**a.

Tomograms of this cylinder arrangement are obtained both with and without SC shells (we use 180 projections). Very similar results are obtained for the Born and Rytov approximations. The tomograms for the latter are shown in Figure 6b, from which we observe that the bare cylinders are hardly distinguishable, and can be mistaken for a single object (they appear as a cylinder of radius 2λ along the central line, as can be seen in Figure 6c). On the contrary, the tomogram of the cloaked cylinders shows two clearly separate profiles, as seen in Figure 6b, even though they are touching each other, which is a remarkable feature. This fact, combined with the enhanced range between the minimum and

The simulation of the electric field at f_0 for this configuration is shown in **Figure 7**a.

To compare the detection sensibility of the SCS and DT approaches, we study the frequency range from $0.98f_0$ to $1.016f_0$, initially considering a lossless material ($\gamma = 0$). We take 1000 projections over a detector with a length $w_D = 100\lambda_0$ and sample the field of each projection at 1000 points. The tomogram of the un-cloaked object is depicted in Figure 7c, which, as seen in Figure 7d, exhibits the typical ripple that arises when tomography is applied over a large circular object.[18] In line with the results reported in refs. [7, 23] Figure 7b shows that the curve representing O_{SCS} as a function of frequency has a V shape, with a spectral region around f_0 where the SCS of the cloaked configurations is lower than that produced by the bare object. Beyond these limits, the cloaked object scatters more energy than the bare one (values greater than 0 dB in Figure 7b). Although the device was designed to have ideal parameters at f_0, the minimum of O_{SCS} is achieved at $f = 0.998f_0$. This slight change may be due to the numerical error introduced by the simulation software.

The relative observability obtained with DT is also depicted in Figure 7b, showing a minimum approximately at f_0 and the same trend as the O_{SCS} curve. However, the mentioned low observability region found in the SCS analysis is considerably narrowed when using DT for both the Born and the Rytov approximations. Moreover, $O_{DT} > O_{SCS}$ in almost all the analyzed spectrum (especially a frequencies below f_0), confirming that DT is more sensitive to lossless realistic cloaks than SCS measurements.

To understand this behavior, the Rytov tomograms of the cloaked object at five different frequencies (indicated by colored dots in Figure 7b) are shown in Figure 7c. The RI values of these tomograms along a line passing through the center of the cloak are depicted in Figure 7d. The Born approximation gives similar results and is not shown. The effect of the cloak in the scattered field at the frequency for which O_{DT} reaches its lowest value (yellow line in Figure 7d) gives rise to a tomogram that corresponds to a thinner object than the original one (as in the SC case) and with RI values below n_{BG}. As a consequence, while the presence of the cloaked object is quite reduced with respect to that of the uncloaked object, this makes $O_{DT} > O_{SCS}$ at f_0. As might be expected, the detection is more precise at frequencies different from f_0. In particular, the tomograms associated with the other four frequencies show a variation of the RI spanning a circular region with approximately the same size as the cloak, thus providing information on the shape of the device (see Figure 7c,d). In addition to these variations, a concentric ripple of the RI is observed for the frequencies that are farther from f_0, that is, $f = 0.989f_0$ (purple line) and $f = 1.012f_0$ (magenta line), which results in higher observability values. The Drude and Lorentz approximations used to model the cloak also allow us to

TO cloak with an x-directed plane wave. b) Comparison between the relative observability of a TO-cloaked dielectric cylinder obtained via SCS and DT. c) Tomograms (Rytov approximation) associated with the non-cloaked cylinder and the cloaked cylinder for different frequencies (corresponding to the color dots in (b)). The size of the tomograms is $16\lambda_0 \times 16\lambda_0$. d) Detail of the RI along the dashed lines depicted in (c). e) Comparison between the relative observability obtained via SCS and the Born and Rytov approximations of DT as a function of the loss order.
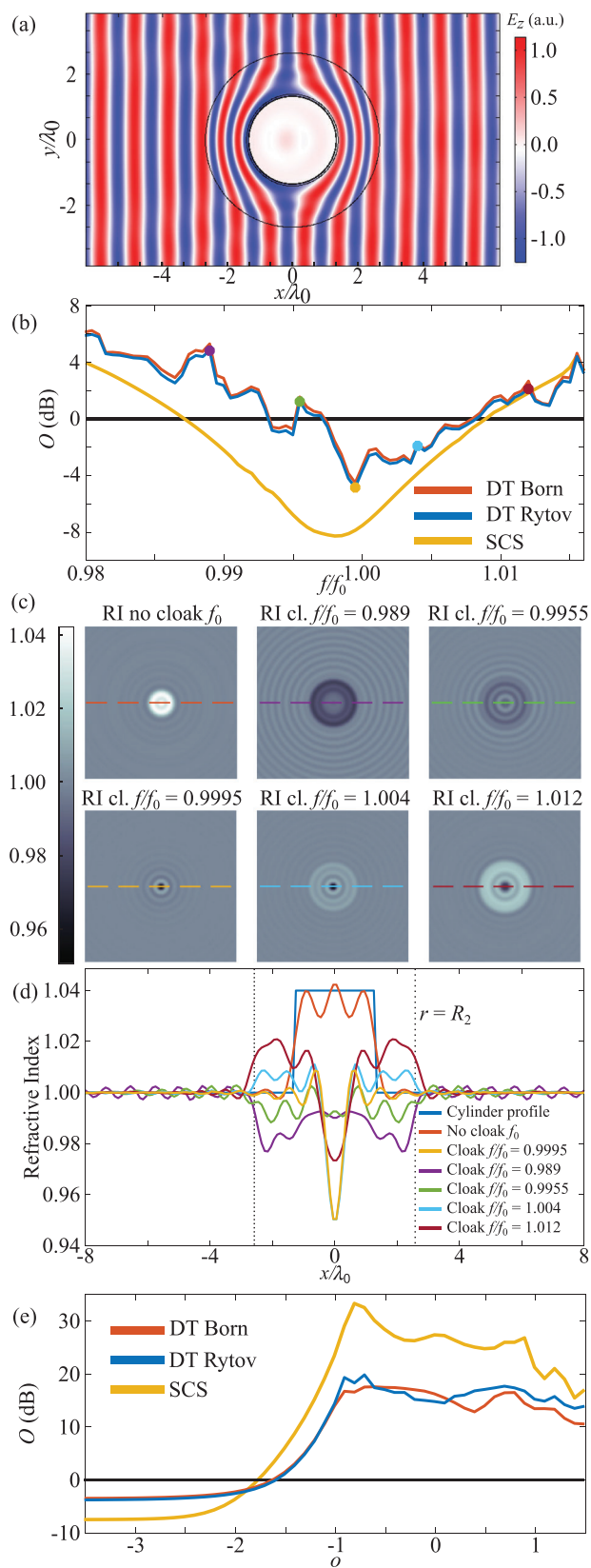
Figure 7. a) Simulated z component of the electric field resulting from the illumination of a dielectric cylinder covered by a lossless dispersive

**ADVANCED
SCIENCE NEWS**

www.advancedsciencenews.com

**LASER
& PHOTONICS
REVIEWS**

www.lpr-journal.org

study the impact of losses in the detection. To this end, we relate γ to the design frequency as follows

$$\gamma = 10^o f_0 \qquad (9)$$

where o is termed the loss order. A high value of o will be related to a high value of loss. We sweep the value of o from -3.5 to 1.5 (keeping the frequency constant at f_0) and show the corresponding observability in Figure 7e. For low losses, the results correspond to the values in Figure 7b at $f = f_0$. However, the SCS becomes more sensitive than DT for $o > -1.9$ (note that this corresponds to a material with considerably high loss values, not usually employed to construct cloaks). Interestingly, the maximum values of the observability are achieved around $o = -1$. For $o > 1$, the observability associated with the SCS and DT methods has similar values.

2.3. Transformation Optics - Polygonal Cloaks

The practical implementation of the ideal TO invisibility cloak studied in the previous section is challenging due to the inhomogeneous character of the ϵ and μ tensors, as well as to the extreme values of these tensors near the inner limits of the cloak. One way to address this drawback is to apply a piecewise affine transformation to a polygonal region divided into segments, which results in a homogeneous device with finite constitutive parameters.[24] A simplified version of this cloak can even be implemented with natural birefringent crystals. Moreover, the study of this kind of device allows us to test the DT detection ability for cloaks with non-cylindrical shapes. In particular, here we consider a hexagonal cloak (the details of which are shown in Figure 2c as an example) and a square cloak, following the transformations reported in refs. [24, 25] respectively. In the case of the hexagonal cloak, the employed dimensions are $r_2 = 4.8\lambda$, $r_1 = r_2/3$, and $r_0 = 0.03\lambda$. The response of this cloak to a TE plane wave is shown in **Figure 8**a,b for two different angles of illumination (0 and $\pi/6$ rad). As for the square cloak, the inner and outer square boundaries have a side length of 2λ and 8.5λ, respectively. A simulation of its behavior for 0 rad and $\pi/4$ rad illumination angles are shown in Figure 8c,d.

To analyze the behavior of the considered polygonal cloaks under the SCS and DT paradigms, a hexagon and a square with a refractive index $n_{OBJ} = 1.05$ have been placed inside the cloaks ($n_{BG} = 1$). In the case of the hexagonal cloak, the hidden hexagonal object has a radius r_1 and the hidden square has a side length r_1. In the case of the square cloak, the hidden hexagon has a radius of $r = 1.02\lambda$. Through this study, we have verified that, although polygonal invisibility devices work well for any angle of illumination, their performance has a slight angle dependence by construction (the region of virtual space that is expanded is not a point, but a finite domain without cylindrical symmetry). For instance, when the hidden object is the hexagon, O_{SCS} varies from 0.22 in the worst case (angle of illumination of $\pi/6$ rad) to 0.19 when the illumination angle is 0 rad. The SCS ratios for the rest of the cases are gathered in **Table 1**. In all configurations, the SCS is significantly reduced, especially by the square cloak.

The same analysis is now repeated using DT under the Rytov approximation. The tomograms of the two considered bare ob-

jects are shown in Figure 8e and are used as a reference. The tomograms of the different cloak-object combinations can be seen in Figure 8f,g. The values of O_{DT} for each case are shown in Table 1. As seen, the relative observability associated with the DT approach is always significantly higher than that associated with the SCS method, being higher than unity in some cases (meaning that the cloak enhances the presence of the object in the eyes of tomography).

In addition, the tomograms of Figure 8e–g evidence the imaging ability of DT for non-cylindrical cloaks. First, they show a clear correspondence between the size of the retrieved index profile and the outer boundaries of both cloaks. Second, the tomograms possess the same symmetries as the cloaks, as can be seen in Figure 8f,g. Hence, although the hidden objects are not unmasked by the tomograms, the latter provide important information on the cloaking device, revealing its presence. This means that, while small changes in the scattered energy as a function of the illumination angle do not compromise the cloak performance in terms of SCS (with low values of O_{SCS} well below unity in all cases), they are magnified by DT due to the smart combination of the measured complex field at different angles. Therefore, the high values of O_{DT}, together with the ability of DT to determine the shape of the cloak, makes this technique a much better candidate for the identification of this kind of device than the SCS. Furthermore, the most remarkable fact is that this identification has been done at the design frequency of the cloak, that is, for the exact ideal parameters of the device. It is for this reason that we have not carried out a frequency sweep to analyze the spectral dependence of the observability in this case, although one would expect an increment in the values of this parameter as moving away from f_0.

2.4. Beyond the Limits of Tomography Approximations

At this point, it is worth noting that, although the employed DT approach is restricted to isotropic objects possessing a low index gradient, invisibility cloaks do not usually fulfill these conditions. However, our results prove that the considered DT technique also shows a high efficiency when it comes to imaging and detecting cloaks with extreme parameters (such as a negative permittivity in the case of SC cloaks, or as anisotropic rapidly-varying materials in the case of TO cloaks), as well as a high index contrast with either the background or the cloaked object (which is the situation in all the analyzed cases). The key aspect here is that, even when the conditions for the Born and Rytov approximations to be valid are broken, the associated DT algorithms are usually still able to capture the main features of an object. Specifically, although the retrieved RI value may differ from the real one, strong variations in the optical properties of the object are reflected in the tomogram,[18,26,27] enabling us to still detect the presence of the object. Following this idea, in this section we analyze the case in which the cloaked object does not fulfill the validity conditions of the Born and Rytov approximations.

We start by studying the SC technique. In this case, we selected an optimized cloak design from ref. [8]. The RI of the cloaked cylinder is $\sqrt{3}$, which is in sharp contrast to n_{BG} and far away from the aforementioned 5% limit. Moreover, the radius of the
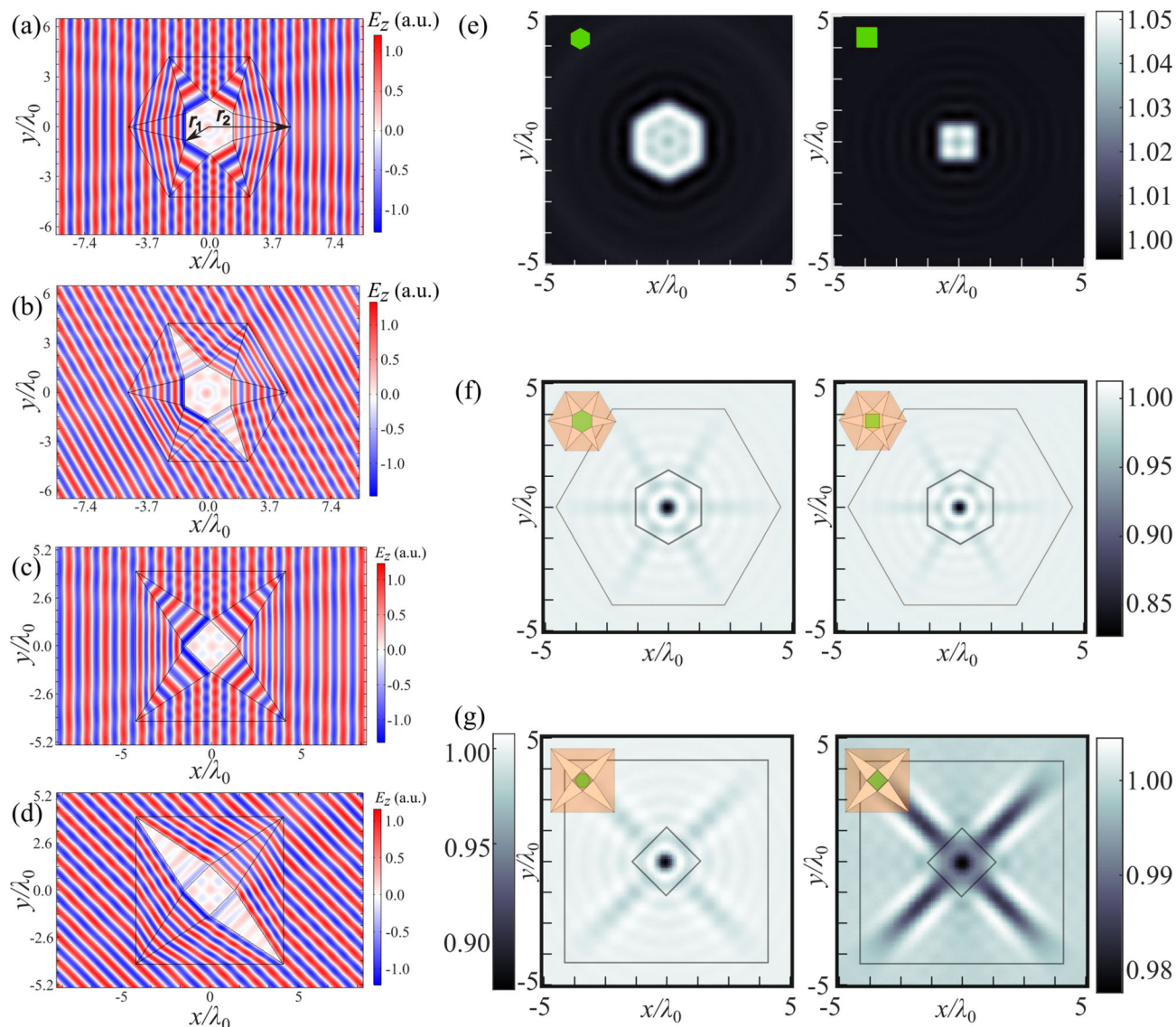
Figure 8. a–d) Simulated z component of the electric field resulting from the illumination of different polygonal TO cloaks with an x-directed plane wave. Hexagonal cloak illuminated at an angle of 0 rad (a) and hexagonal cloak illuminated at an angle of $\pi/6$ rad (b). Square cloak illuminated at an angle of 0 rad (c). Square cloak illuminated at an angle of $\pi/4$ rad (d). e–g) Tomograms (Rytov approximation) of: a bare hexagon and a bare square (e). Each of these objects hidden within a hexagonal cloak (f) and within a square cloak (g). The boundaries of the cloaks are depicted as a reference. The schematic insets represent the cloak (pink) and the hidden object (green) for each configuration.

Table 1. SCS and DT (Rytov) relative observability for each cloak-object combination (H: Hexagonal, S: Square).

Cloak	Object	O_{SCS}	O_{DT}
H	H	0.22–0.19	0.74
H	S	0.52–0.47	1.69
S	H	0.40–0.18	1.51
S	S	0.13–0.05	0.81

cylinder is $r = \lambda_0/7.8$, which is well below the diffraction limit we imposed above. **Figure 9**a,b shows the tomograms of the bare and cloaked cylinder. As expected, the reconstructed RI of the bare cylinder is significantly lower than the original one due to the employed Rytov approximation. Moreover, the radius of the cylinder retrieved by DT has been widened as compared to the real one, since any object with a size below the diffraction limit will appear as an object with a size of the order of this limit, as in typical far-field imaging. It is worth mentioning that this result could be improved by using advanced nonlinear DT approaches that are able to overcome the diffraction limit by up to an order of magnitude.[28] In any case, as seen, the cylinder is still detected even when surrounded by the cloak. Moreover, while the cloak behaves excellently in terms of SCS ($O_{SCS} = -9$ dB), DT considerably improves the observability to $O_{DT} = -3$ dB. That is, DT is also effective in detecting standard electrically small SC cloaks with a high RI contrast.
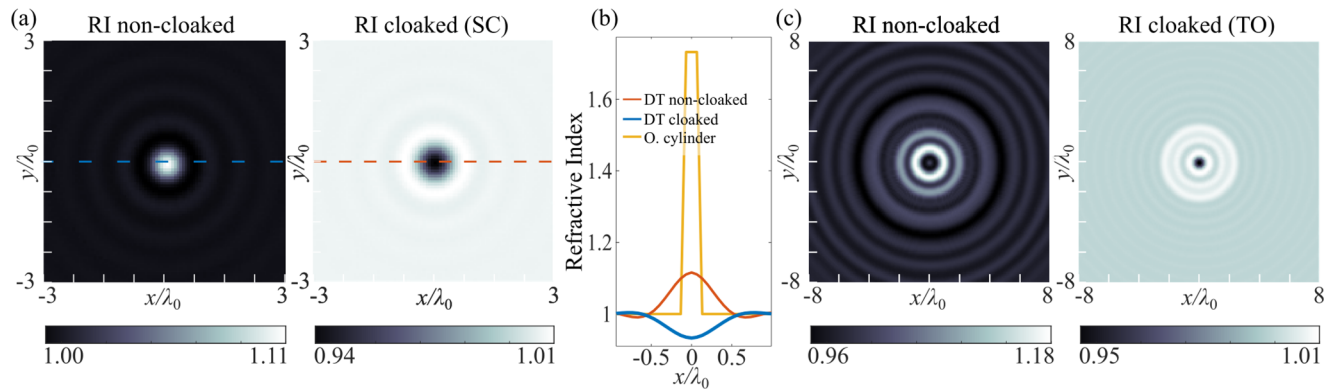
Figure 9. a,b) Linear tomography (Rytov approximation) of a non-cloaked and cloaked dielectric cylinder (scattering cancellation) of radius $r = \lambda_0/7.8$ at $f = f_0$. Full tomograms are shown in panel (a). Panel (b) shows a detail of the RI along the dashed lines depicted in (a). c) Tomograms (Rytov approximation) associated with the non-cloaked and cloaked cylinders (transformation optics) at $f = 1.004 f_0$.

As a second example, we test the ability of our technique to detect the TO cloak analyzed in Section 2.2 when hiding a strong scatterer with a RI of 2. In this case, the tomogram of the cloaked object returns the same RI distribution as in Section 2.2, correctly predicting the size and shape of the cloak once again (Figure 9c). The reason for this equality is that the TO cloak prevents the incident field from entering the cloaked space, making the scattered field almost independent of the cloaked object. Hence, DT allows us to retrieve the shape, size, and position of TO cloaks regardless of the concealed object. Moreover, even though the estimated RI value of the bare scatterer is again considerably below its real value due to the broken Rytov approximation, the DT observability remains better ($O_{DT} = -9.4$ dB) than in the SCS case ($O_{SCS} = -12.5$ dB).

Finally, it is important to highlight that the typical approximations considered in DT are not a necessary requirement of this technique, but rather an ingredient that simplifies the inversion of the equations. In particular, both the Born and Rytov approximations, which limit the space of objects whose RI distributions can be obtained accurately to weak scatterers, consist of keeping only the first term of a series expansion of the field. However, one can consider any number of terms to arbitrarily increase the accuracy of DT in estimating the scatterer RI distribution.[29] A variety of other alternative approaches can also go beyond the Born and Rytov approximations, based on, for example, acquiring tomograms at multiple depths,[30] the method of very fast simulated annealing,[31] a combination of advanced forward and inverse problem solvers,[32] deep learning,[33] and other nonlinear inversion techniques.[34,35] In this way, it is possible to overcome the restrictions of the first-order Born and Rytov approximations and precisely obtain the index profile of strong scatterers and multiple scattering objects via DT. Therefore, approximations are not an inherent drawback of DT. Nonetheless, we have used the Born and Rytov approximations due to their simplicity and common use in the literature, as they already allow us to obtain remarkable results not attainable by previous approaches, such as the possibility of retrieving the shape and size of a cloak, as well as the associated improvement in the sensitivity to detect its presence. This provides a proof of concept of the potential of DT in invisibility device detection that will hopefully stimulate further research efforts aimed at refining it. Along this line, we would

like to reiterate that a key aspect in DT is that the information provided by the phase and distribution of the scattered field allows us to unambiguously retrieve the optical properties of the scatterer under certain conditions.[36] On the contrary, the information provided by the SCS is highly ambiguous in nature, meaning that the same SCS can be produced by objects with a different location, shape, size, or refractive index level (or combinations of these). DT removes this ambiguity by measuring the field amplitude and phase distributions (for several illumination angles if one has to account for objects without rotational symmetry) and by combining them in a specific way,[37] more insightful than the one in which the SCS does it.

3. Conclusion

In this work, we have studied the potential offered by diffraction tomography for the detection of realistic invisibility devices. In this direction, we have shown that this technique is more sensitive than the broadly used scattering cross-section for cloaks based on both scattering cancellation and transformation optics around the design frequency of these devices. Moreover, diffraction tomography can approximately reveal the shape and the size of all the analyzed devices.

More specifically, regarding scattering cancellation cloaks and blow-up-a-point transformation optics cloaks, the presence of the cloaked object has been compared to that of the uncloaked one for different frequencies, finding that the band at which the system possesses low observability according to a scattering cross-section meter ($O_{SCS} < 1$) is notably reduced for the diffraction tomography technique, the observability of the system being always higher or equal under a diffraction tomography analysis ($O_{DT} \geq O_{SCS}$). In addition, while polygonal transformation optics cloaks have been verified to do a good job in hiding objects as far as the scattering cross-section parameter is concerned, diffraction tomography is able to image the shape of these cloaks and can therefore reveal their presence, compromising their effectiveness. Remarkably, this occurs for the ideal cloak parameters.

Since diffraction tomography represents a more demanding test for the performance evaluation of invisibility cloaks, it might be useful as a new standard in their design and characterization. Additionally, our findings open up a range of potential benefits

in a variety of fields, from fundamental advances in invisibility research to bioimaging and warfare applications at the technological level.

Besides, our results indicate that objects cloaked using scattering cancellation appear to be shrunk from a tomographic point of view. This suggests that the scattering cancellation technique could be applied to enhance the resolution of diffraction tomography when imaging small closely-packed particles.

The study is concluded by analyzing the performance of the proposed technique beyond the first-order Born and Rytov approximations, still proving to be superior to the SCS approach.

To complete the discussion, we would like to make a note about the robustness of the proposed method. First, it shows a high tolerance to deviations in the considered approximations and diffraction tomography assumptions, as discussed in the previous section. Second, although we have employed a high number of projections to obtain the tomograms in this work, a much lower number would be enough in some cases. For instance, the reported polygonal cloak tomograms were obtained using a number of projections ranging from 180 to 360. However, the shape of the cloak can be distinguished even with only a few tens of projections. In any case, one also has to take into account that the diffraction tomography reconstruction error decreases with the number of considered illumination angles until it stabilizes at a constant value.[13] Another important source of error in diffraction tomography is the noise introduced by the use of highly coherent light, which is strengthened by the reconstruction algorithm. Fortunately, there exist different approaches to suppress this noise, based on deep learning and other techniques.[38,39]

Finally, given the analogy between optics and acoustics, as well as the advanced state of sonic diffraction tomography,[40,41] the proposed technique could be easily extended to the detection of sound cloaks.[42,43]

Experimental Section

Scattering Cross Section (SCS): To evaluate the rate of the electromagnetic energy that was scattered by a particle, the scattering cross-section[44] is defined as

$$SCS = \frac{W_{SCA}}{P_{INC}} \qquad (10)$$

where P_{INC} is the incident irradiance, defined as energy flux of the incident wave (W m^{-1}). W_{SCA} is the scattered energy rate (W), which, in 2D, is derived by contour integration of the Poynting vector associated with the scattered field ($\mathcal{P}_{SCA}$) over a circumference enclosing the particle (L)

$$W_{SCA} = \oint_L \mathcal{P}_{SCA} \cdot \hat{\mathbf{n}} \, dl \qquad (11)$$

where $\hat{\mathbf{n}}$ is the unit vector normal to L. In the present work, all electromagnetic field and SCS calculations were performed in COMSOL MULTIPHYSICS.

Conflict of Interest

The authors declare no conflict of interest.

Data Availability Statement

The data that support the findings of this study are available from the corresponding author upon reasonable request.

[1] N. Engheta, R. W. Ziolkowski, *Metamaterials: Physics and Engineering Explorations*, Wiley, Hoboken, NJ **2006**.

[2] A. Alù, N. Engheta, *Phy. Rev. E* **2005**, *72*, 016623.

[3] J. B. Pendry, D. Schurig, D. R. Smith, *Science* **2006**, *312*, 1780.

[4] D. Schurig, J. J. Mock, B. J. Justice, S. A. Cummer, J. B. Pendry, A. F. Starr, D. R. Smith, *Science* **2006**, *314*, 977.

[5] D. Rainwater, A. Kerkhoff, K. Melin, J. C. Soric, G. Moreno, A. Alù, *New J. Phys.* **2012**, *14*, 013054.

[6] M. Kadic, T. Bückmann, R. Schittny, M. Wegener, *Philos. Trans. A Math. Phys. Eng. Sci.* **2015**, *373*, 20140357.

[7] F. Monticone, A. Alù, *Phys. Rev. X* **2013**, *3*, 041005.

[8] P.-Y. Chen, J. Soric, A. Alù, *Adv. Mater.* **2012**, *24*, OP281.

[9] F. Monticone, A. Alù, *Optica* **2016**, *3*, 718.

[10] A. Greenleaf, M. Lassas, G. Uhlmann, *Physiol. Meas.* **2003**, *24*, 413.

[11] A. J. Devaney, *Ultrason. Imaging* **1982**, *4*, 33.

[12] P. Müller, M. Schürmann, J. Guck, *arXiv:1507.00466*, **2016**.

[13] P. Müller, M. Schürmann, J. Guck, *BMC Bioinf.* **2015**, *16*, 367.

[14] M. Schürmann, G. Cojoc, S. Girardo, E. Ulbricht, J. Guck, P. Müller, *J. Biophotonics* **2017**, *11*, 201700145.

[15] F. Gömöry, M. Solovyov, J. Souc, C. Navau, J. Prat-Camps, A. Sanchez, *Science* **2012**, *335*, 1466.

[16] R. Schittny, M. Kadic, T. Bückmann, M. Wegener, *Science* **2014**, *345*, 427.

[17] A. Alù, N. Engheta, *Phys. Rev. Lett.* **2009**, *102*, 233901.

[18] B. Chen, J. J. Stamnes, *Appl. Opt.* **1998**, *37*, 2996.

[19] M. G. Silveirinha, A. Alù, N. Engheta, *Phys. Rev. E* **2007**, *75*, 036603.

[20] P. B. Johnson, R. W. Christy, *Phy. Rev. B* **1972**, *6*, 4370.

[21] U. Leonhardt, *Science* **2006**, *312*, 1777.

[22] S. A. Cummer, B.-I. Popa, D. Schurig, D. R. Smith, J. Pendry, *Phys. Rev. E* **2006**, *74*, 036621.

[23] B. Zhang, B.-I. Wu, H. Chen, J. A. Kong, *Phys. Rev. Lett.* **2008**, *101*, 063902.

[24] H. Chen, B. Zheng, *Sci. Rep.* **2012**, *2*, 255.

[25] B. Orazbayev, M. Beruete, A. Martínez, C. García-Meca, *Phys. Rev. A* **2016**, *94*, 063850.

[26] M. Slaney, A. C. Kak, L. E. Larsen, *IEEE Trans. Microwave Theory Tech.* **1984**, *32*, 860.

[27] D. Rajan, G. V. Frisk, *Geophysics* **1989**, *54*, 864.

[28] J. Girard, G. Maire, H. Giovannini, A. Talneau, K. Belkebir, P. C. Chaumet, A. Sentenac, *Phys. Rev. A* **2010**, *82*, 061801(R).

[29] G. A. Tsihrintzis, A. J. Devaney, *IEEE Trans. Image Process.* **2000**, *9*, 1560.

[30] W. Choi, C. Fang-Yen, K. Badizadegan, R. R. Dasari, M. S. Feld, *Opt. Lett.* **2008**, *33*, 171.

[31] M. Mahapatra, S. Mahapatra, *J. Appl. Geophys.* **2009**, *2*, 125.

[32] J. Wiskin, D. T. Borup, S. A. Johnson, M. Berggren, *J. Acoust. Soc. Am.* **2012**, *131*, 3802.

[33] J. Lim, A. B. Ayoub, E. E. Antoine, D. Psaltis, *Light: Sci. Appl.* **2019**, *8*, 82.

[34] Y. M. Wang, W. C. Chew, *Int. J. Imaging. Syst. Technol.* **1989**, *1*, 100.

[35] W. C. Chew, G. P. Otto, W. H. Weedon, J. H. Lin, C. C. Lu, Y. M. Wang, M. Moghaddam, *Int. J. Imaging. Syst. Technol.* **1996**, *7*, 16.

[36] E. Wolf, *J. Opt. Soc. Am.* **1970**, *60*, 18.

[37] E. Wolf, *Opt. Commun.* **1969**, *1*, 153.

[38] J. Kostencka, T. Kozacki, M. Dudek, M. Kujawinska, *Opt. Express* **2014**, *22*, 5731.

[39] G. Choi, D. H. Ryu, Y. J. Jo, Y. S. Kim, W. Park, H. Min, Y. K. Park, *Opt. Express* **2019**, *27*, 4927.

[40] O. M. Gaddoura, M. Ding, *Int. J. Manuf. Eng.* **2011**, *1*, 10.

[41] N. Ozmen, R. Dapp, M. Zapf, H. Gemmeke, N. V. Ruiter, K. W. van Dongen, *IEEE Trans. Ultrason. Ferroelect. Freq. Control* **2015**, *62*, 637.

[42] A. N. Norris, *Acoust. Today* **2015**, *11*, 38.

[43] S. A. Cummer, J. Christensen, A. Alù, *Nat. Rev. Mater.* **2016**, *1*, 16001.

[44] S. Yushanov, J. S. Crompton, K. C. Koppenhoefer, in *Proc. of the COMSOL Conference*, COSMOL, Boston, USA **2013**.

2200237 (11 of 11)